

Article pubs.acs.org/JACS

# Hydrogen Evolution Electrocatalyst Design: Turning Inert Gold into Active Catalyst by Atomically Precise Nanochemistry

Yingwei Li,<sup>\$</sup> Site Li,<sup>\$</sup> Anantha V. Nagarajan,<sup>\$</sup> Zhongyu Liu, Sarah Nevins, Yongbo Song,\* Giannis Mpourmpakis,\* and Rongchao Jin\*



-0.6

ABSTRACT: Electrocatalytic hydrogen evolution reaction (HER) holds promise in the renewable clean energy scheme. Crystalline Au and Ag are, however, poor in catalyzing HER, and the ligands on colloidal nanoparticles are generally another disadvantage. Herein, we report a thiolate (SR)-protected Au<sub>36</sub>Ag<sub>2</sub>(SR)<sub>18</sub> nanocluster with low coverage of ligands and a core composed of three icosahedral  $(I_b)$  units for catalyzing HER efficiently. This trimeric structure, together with the monomeric  $I_b$  Au<sub>25</sub>(SR)<sub>18</sub> and dimeric  $I_h$  Au<sub>38</sub>(SR)<sub>24</sub>, constitutes a unique series, providing an opportunity for revealing the correlation between the catalytic properties and the catalyst's structure. The Au<sub>36</sub>Ag<sub>2</sub>(SR)<sub>18</sub> surprisingly exhibits high catalytic activity at lower overpotentials for HER due to its low ligand-to-metal ratio, low-coordinated Au atoms and unfilled superatomic orbitals. The current density of Au<sub>36</sub>Ag<sub>2</sub>(SR)<sub>18</sub> at -0.3 V vs RHE is 3.8 and 5.1 times that of Au<sub>25</sub>(SR)<sub>18</sub> and Au<sub>38</sub>(SR)<sub>24</sub>, respectively. Density functional theory (DFT) calculations reveal lower hydrogen binding energy and higher electron affinity of Au<sub>36</sub>Ag<sub>2</sub>(SR)<sub>18</sub> for an energetically feasible HER pathway. Our findings provide a new strategy for constructing highly active catalysts from inert metals by pursuing atomically precise nanoclusters and controlling their geometrical and electronic structures.

## INTRODUCTION

Noble metal Pt and its alloy nanoparticles (NPs) are considered to be the most promising catalysts for hydrogen evolution reaction  $(HER)^{1-3}$  with large cathodic current densities at low overpotentials. Recently, non-noble, earthabundant metals are also studied for electrochemical HER.4-Gold and silver are unfortunately less active in the HER process due to high free energy of hydrogen (\*H) adsorption and low current densities. 8,9 The size regime between conventional Au (or Ag) NPs and organometallic complexes gives rise to nanoclusters (NCs) consisting of dozens to hundreds of metal atoms per particle. Recent progress has led to atomic precision for 1-3 nm metal NCs protected by organic ligands (e.g., thiolate (SR)). 10 This emergent class of nanomaterials provides unprecedented opportunities for relating the atomic-level structures to various properties, 11-14 as the total structures of NCs can be revealed by single crystal X-ray diffraction (SCXRD). Such NCs possess much higher surface-to-volume ratios than regular NPs and are thus

-20

-0.2 -0.1 E / V vs. RHE

potentially promising catalysts for H<sub>2</sub> evolution, but they have not been widely applied due to the inert nature of Au and Ag from previous work with regular NPs.3 In recent work, doping Pt/Pd into Au<sub>25</sub>(SR)<sub>18</sub> was found to improve the HER performance compared to the homogold counterpart, 18,19 but Ag doping showed an adverse effect.

To design effective HER catalysts based on Au and Ag, much effort has been put in controlling the structures of NCs, for example, fusion of 13-atom icosahedral building blocks into a linear dimer or trimer. 21,22 Trimeric NCs often exhibit outstanding electronic and optical properties.<sup>23</sup> We aim at obtaining NCs with more exposed surface metal atoms for \*H

Received: May 3, 2021 Published: July 16, 2021





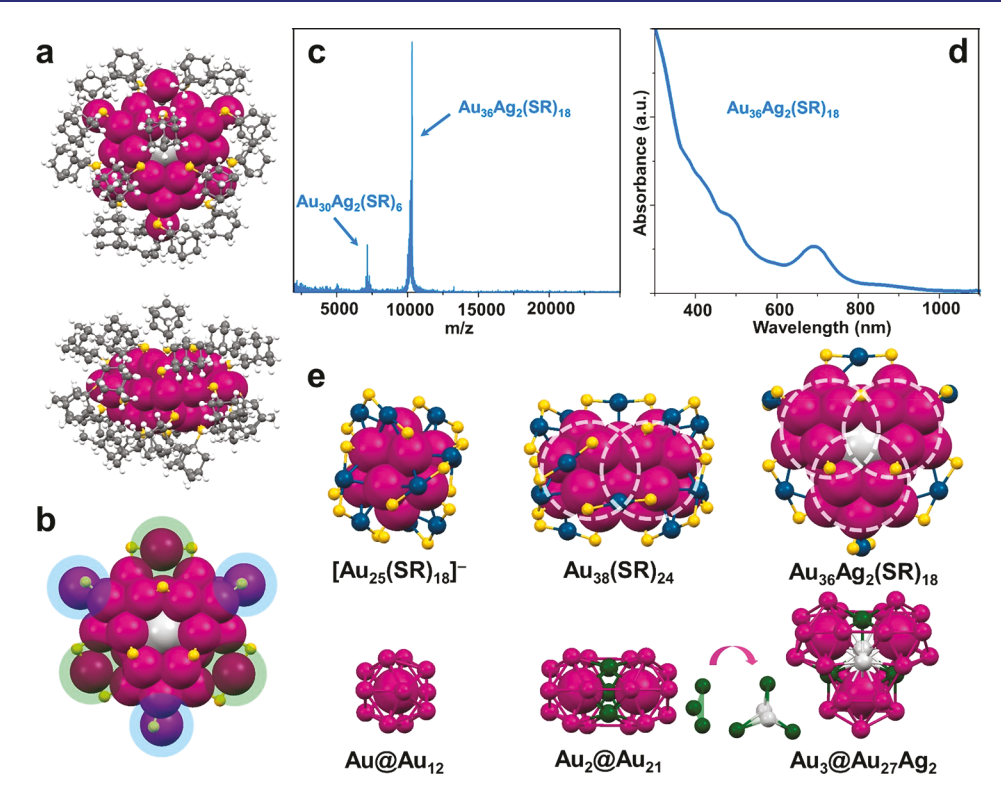


**Figure 1.** (a) The total structure (top and side views) of  $Au_{36}Ag_2(SR)_{18}$  NC. (b) The carbon tail-omitted  $Au_{36}Ag_2S_{18}$  structure: the Au atoms of  $Au(SR)_2$  motifs on each  $I_h$  unit are indicated by blue circles; whereas the Au atoms of  $Au(SR)_2$  motifs that bridge two  $I_h$  units are indicated by green circles. (c) MALDI-MS spectrum and (d) UV-vis spectrum of  $Au_{36}Ag_2(SR)_{18}$  NCs; note that  $Au_{30}Ag_2(SR)_6$  in the mass spectrum is a fragment. (e) The Au-S structures (top) and kernel structures (bottom) of monomeric  $I_h$   $[Au_{25}(SR)_{18}]^-$  (left), dimeric  $I_h$   $Au_{36}(SR)_{24}$  (middle), and trimeric  $I_h$   $Au_{36}Ag_2(SR)_{18}$  (right), each dashed circle indicates one  $I_h$  unit. Color codes: a and b, magenta = Au, light gray = Ag, yellow = S, gray = C, and white = H; e, magenta/green = kernel Au, navy = motif Au, light gray = Ag, and yellow = S.

adsorption via atomically precise nanochemistry to design an effective Au/Ag catalyst for HER, even though the catalyst is composed of traditionally inactive metals.

Herein, we report a success in synthesizing a trimeric  $Au_{36}Ag_2(SR)_{18}$  NC in which three icosahedral  $(I_h)$  units are face-fused together in a cyclic manner. A series of NCs, i.e., monomeric Au<sub>25</sub>(SR)<sub>18</sub>-, dimeric Au<sub>38</sub>(SR)<sub>24</sub> and trimeric Au<sub>36</sub>Ag<sub>2</sub>(SR)<sub>18</sub>, are thus available for a comparative study in HER and for revealing important insight. The "face-fusion" mode makes the three  $I_h$  building blocks more closely attached to each other, resulting in unfilled supermolecular orbitals (note that the Au<sub>36</sub>Ag<sub>2</sub>(SR)<sub>18</sub> supermolecule comprises three  $I_h$  superatoms), in contrast to the NCs composed of multiple vertex-shared icosahedrons (indicated by the total free-valenceelectron counts to be integer multiples of 8e, i.e., 8e, 16e, 24e). 23,24 As a result, Au<sub>36</sub>Ag<sub>2</sub>(SR)<sub>18</sub> exhibits a much lower onset overpotential for HER and greatly increased current density. This is important as Au and Ag, as well as thiolate ligands are known to be adverse for HER catalysis. 8,9,25 DFT calculations demonstrate that the trimeric NC exhibits favorable hydrogen formation thermodynamics and a higher electron affinity compared to the monomeric and dimeric NCs. Thus, tailoring the geometrical and electronic structures of atomically precise Au/Ag NCs can lead to highly active catalysts for HER.

#### RESULTS AND DISCUSSION

Characterization of Trimeric  $Au_{36}Ag_2(SR)_{18}$ . The  $Au_{36}Ag_2(SR)_{18}$  (where, SR = adamantanethiolate,  $SC_{10}H_{15}$ , Figure 1) NC was synthesized through a coreduction of  $Au^I$ –

 $SC_{10}H_{15}$  and  $Ag^I - SC_{10}H_{15}$  (molar ratio = 10:1) by NaBH<sub>4</sub>, and the product was purified by crystallization (see Supporting Information for details). The crystal structure of  $Au_{36}Ag_2(SR)_{18}$  was solved by SCXRD (Figure 1a/Table S1), which possesses a face-fused tri-icosahedral  $Au_{30}Ag_2$  kernel on which three bridging thiolates connect the three  $I_h$  building blocks on the top and another three thiolates at the bottom. Each  $I_h$  unit is further protected by one  $Au(SR)_2$  motif (Figure 1b, marked in blue shadows, three total), and another  $Au(SR)_2$  motif bridges two  $I_h$  as well (Figure 1b, marked in green shadows, three total). The entire  $Au_{36}Ag_2S_{18}$  structure without the organic tails possesses a quasi- $D_{3h}$  symmetry. The two Ag atoms reside at the  $C_3$  axial positions of the NC, i.e., they are shared by all three  $I_h$  units.

The UV–vis spectrum of  $Au_{36}Ag_2(SR)_{18}$  (in toluene) shows a prominent peak at ~690 nm, with other less pronounced ones at ~380, ~430, ~490, and ~860 nm (Figure 1d), indicating a molecular state of the NC (as opposed to metallic-state NPs). MALDI mass spectrometry (MS) shows an intense peak corresponding to  $Au_{36}Ag_2(SR)_{18}$  (Figure 1c) as well as a weak peak for the  $Au_{30}Ag_2(SR)_{6}$  fragment, and the difference between these two peaks is the mass loss of  $Au_6(SR)_{12}$  fragment, which is consistent with the six  $Au(SR)_2$  motifs on the surface of the kernel; note that in the MS spectrum (Figure S1), a weaker peak representing  $Au_{35}Ag_3(SR)_{18}$  was also detected; however, the crystal data does not show any third Ag atom in the structure. Thus, the  $Au_{35}Ag_3(SR)_{18}$  byproduct should be decomposed during the crystallization, leaving pure  $Au_{36}Ag_2(SR)_{18}$ .

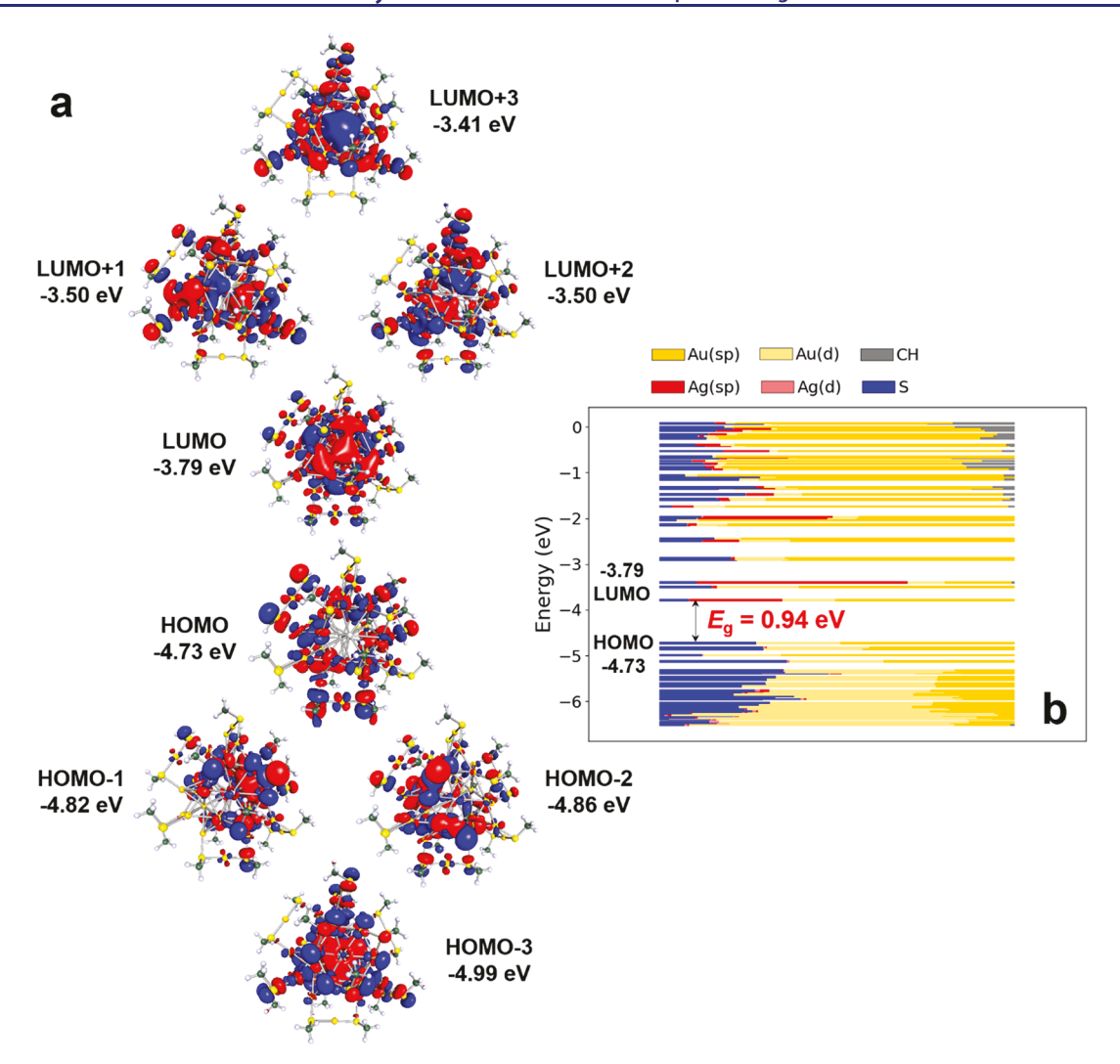


Figure 2. (a) Visualized frontier molecular orbitals of  $Au_{36}Ag_2(SCH_3)_{18}$  and their corresponding energy levels. (b) KS orbital energy level diagram for  $Au_{36}Ag_2(SCH_3)_{18}$  with contributions from various atomic-orbitals of Au, Ag, S, C and H.

The obtained  $Au_{36}Ag_2(SR)_{18}$  NC fulfills an interesting series of face-fusion NCs, including the mono- $I_h$  [ $Au_{25}(SR)_{18}$ ]<sup>-,26</sup> bi- $I_h$   $Au_{38}(SR)_{24}$ , and tri- $I_h$   $Au_{36}Ag_2(SR)_{18}$  (Figure 1e). In the bi- $I_h$   $Au_2@Au_{21}$  kernel of  $Au_{38}(SR)_{24}$ , the two  $Au_{13}$  units are face-fused at the middle  $Au_3$  triangle (Figure 1e, middle, marked in green); in the tri- $I_h$   $Au_3@Au_{27}Ag_2$  kernel of  $Au_{36}Ag_2(SR)_{18}$ , three  $Au_{11}Ag_2$  units are face-fused at the central  $Au_3Ag_2$  three-pointed star (Figure 1e, right, marked in green/light gray).

**DFT Calculations on Electronic Structures.** Mulliken contribution is an effective means to illustrate the Kohn–Sham (KS) molecular orbitals at the atomic level. Herein, similar behavior is found for the series of NCs, that is, the highest occupied molecular orbitals (HOMO) of the mono- $I_h$  [Au<sub>25</sub>(SCH<sub>3</sub>)<sub>18</sub>]<sup>-</sup>, bi- $I_h$  Au<sub>38</sub>(SCH<sub>3</sub>)<sub>24</sub>, and tri- $I_h$  Au<sub>36</sub>Ag<sub>2</sub>(SCH<sub>3</sub>)<sub>18</sub> NCs are mainly localized on the central atom(s) in each  $I_h$  (Figure S2/S3, darker red). In contrast, the lowest unoccupied molecular orbitals (LUMO) are mainly distributed on the mono- $I_h$  Au<sub>12</sub> and bi- $I_h$  Au<sub>21</sub> shells (Figure S2, darker blue). As for the Au<sub>36</sub>Ag<sub>2</sub>(SCH<sub>3</sub>)<sub>18</sub>, although its LUMO is also on the tri- $I_h$  Au<sub>27</sub>Ag<sub>2</sub> shell, the orbital density is more localized on the two doping Ag atoms (Figure S3a, darker blue). This observation indicates that for the NC series, the HOMO states are primarily decided by the  $I_h$  central

atom(s), whereas the LUMO states depend more on the  $I_h$ shell atoms. In the newly obtained trimeric Au<sub>36</sub>Ag<sub>2</sub>(SR)<sub>18</sub>, we tried to dope as few heteroatoms as possible, and the controlled doping amount of Ag was proved to be critical in tailoring the structures of atomically precise NCs.<sup>29</sup> The two Ag atoms are thus important to achieve the trimeric structure in the synthesis, and according to DFT (Figure 2), LUMO and especially LUMO+3 orbitals are localized 30 on the two Ag atoms (Figure 2b) which are shared by the three  $I_h$  units, compared to the remaining 27 Au atoms in the tri- $I_h$  shell. We rationalize that the Ih central atom (Au) would take more electron density than the  $I_h$  shell atoms as indicated by Bader charge analysis.  $^{28}$  As a result, the three  $I_h$  centers in the tri- $I_h$ structure would attract more charges and the two axial positions shared by three units should contribute more electron density to the  $I_h$  centers. Thus, the much less electronegative Ag atoms (electronegativity  $\chi_{\rm Ag}$  = 1.93 vs  $\chi_{\rm Au}$  = 2.54) are preferred at these  $C_3$  axial positions.

In DFT calculations, we further replaced the two Ag atoms with Au to obtain a hypothetical trimeric Au<sub>38</sub>(SCH<sub>3</sub>)<sub>18</sub> NC (Figure S3b) to highlight the specific Au atoms at the Ag positions (i.e., Au substitution for Ag) in the KS diagram. One can observe that the two Au atoms still contribute significantly to LUMO and LUMO+1. Accordingly, the KS diagrams of

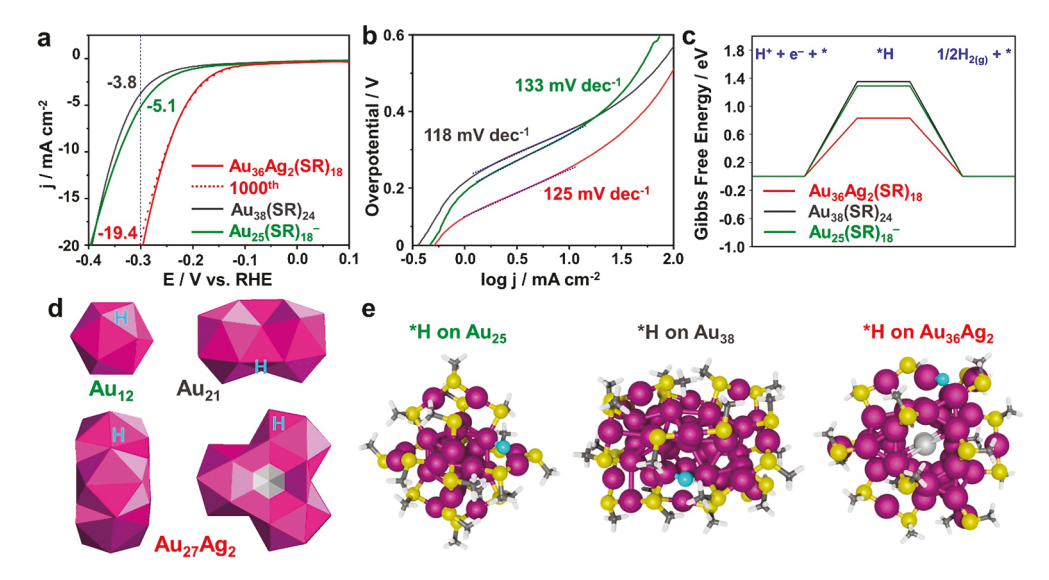


Figure 3. (a) HER voltammograms of NC catalysts. (b) Tafel plots of NC catalysts. (c) Calculated Gibbs free energy of  $H_2(g)$  formation (HER pathway) on the NC catalysts. (d) Illustrated kernel surfaces of NC catalysts for hydrogen adsorption. (e) Relaxed structures of the NCs upon hydrogen adsorption on Au active site. Color codes: magenta = Au, light gray = Ag, yellow = S, cyan = adsorbed H, gray = C, and white = H.

 ${\rm Au_{36}Ag_2(SCH_3)_{18}}$  and  ${\rm Au_{38}(SCH_3)_{18}}$  demonstrate a similar energy for the HOMO, while the replacing Au atoms result in a more negative energy for the LUMO and hence, a 0.15 eV smaller energy gap in  ${\rm Au_{38}(SR)_{18}}$  (Figure S4). The smaller gap might be related to a less stable electronic configuration of homogold trimeric  ${\rm Au_{38}(SR)_{18}}$  which is yet to be synthesized.

The free valence electron number is important for the electronic configuration of superatomic NCs. The number increases from 8e (25-18+1=8) for the monomeric  $[Au_{25}(SR)_{18}]^-$  to 14e (38-24=14) for the dimeric  $Au_{38}(SR)_{24}$  (resembling a diatomic supermolecule), then to 20e (36+2-18=20) for the trimeric  $Au_{36}Ag_2(SR)_{18}$  (a triatomic supermolecule), with a 6e interval, indicating that face-fusion in the kernel makes the supermolecular orbitals electronically nonclosing, i.e., there are unfilled supermolecular orbitals in  $Au_{38}$  and  $Au_{36}Ag_2$  NCs.

DFT calculations are further performed to reveal the electronic structure of Au<sub>36</sub>Ag<sub>2</sub>(SCH<sub>3</sub>)<sub>18</sub> near the HOMO-LUMO gap. The KS diagrams clearly demonstrate the trimeric electronic structure of the molecular orbitals (Figure 2a). The LUMO+1 and LUMO+2 orbitals are degenerate, and the energy levels of HOMO-1 and HOMO-2 are also very close to each other. As no existing triatomic molecule has a cyclic structure, we cannot find an isoelectronic analogue. Nevertheless, the lobes of the molecular orbitals of  $Au_{36}Ag_2(SCH_3)_{18}$ remind us of BF<sub>3</sub> (Figure S5); the  $D_{3h}$  symmetric BF<sub>3</sub> molecule (24e) is not isoelectronic to  $Au_{36}Ag_2(SCH_3)_{18}$  (20e). However, it is interesting to note that the HOMO-3 to LUMO+3 frontier orbitals of Au<sub>36</sub>Ag<sub>2</sub>(SCH<sub>3</sub>)<sub>18</sub> are comparable to those of BF<sub>3</sub>, except the order of LUMO+1/+2 and LUMO+3 energy levels. The order shift is similar to that in the comparison between Au<sub>38</sub>(SR)<sub>24</sub> and its isoelectronic F<sub>2</sub> molecule.32

**Hydrogen Evolution Reaction.** Although Au and Ag are generally poor in HER catalysis, the  $Au_{36}Ag_2(SR)_{18}$  NC with low ligand coverage (*vide infra*) motivated us to test its HER performance. Indeed,  $Au_{36}Ag_2(SR)_{18}$  gives rise to a muchenhanced activity in the HER (Figure 3a), manifested in (1) the onset overpotential of  $Au_{36}Ag_2(SR)_{18}$  to generate  $H_2$  is  $\sim 0.1$  V smaller than that of  $Au_{25}(SR)_{18}^-$  and  $Au_{38}(SR)_{24}$  and

(2) the mass activity of the trimetric NC at an applied voltage of  $-0.3~V~vs~RHE~is~-19.4~mA~cm^{-2}$ , which is 3.8 times that of  $Au_{25}(SR)_{18}~(-5.1~mA~cm^{-2})$  and 5.1 times that of  $Au_{38}(SR)_{24}~(-3.8~mA~cm^{-2})$ . The Tafel slopes (Figure 3b) of the NC series are determined to be 125, 118, and 133 mV dec^-1 for  $Au_{36}Ag_2(SR)_{18},~Au_{38}(SR)_{24},~and~Au_{25}(SR)_{18}^{-},~respectively.$  These similar values indicate similar surface chemistry and the same rate-limiting (Volmer) step for all these three catalysts.

The catalytic activity of the NC series toward HER was further evaluated by DFT (Figure 3c). Fully ligand-protected Au NCs are typically poor catalysts as they exhibit highly endergonic binding energies (>1.2 eV) for hydrogen (H) adsorption. However, it is evident that fully ligated  $\mathrm{Au_{36}Ag_2(SCH_3)_{18}}$  has a significantly lower binding energy of hydrogen ( $\Delta G = 0.83$  eV, Figure 3c) to form the \*H intermediate than  $\mathrm{Au_{25}(SCH_3)_{18}}^-$  (1.29 eV) or  $\mathrm{Au_{38}(SCH_3)_{24}}$  (1.35 eV).

The electrochemically active surface areas (ECSA) of the NC series were also measured (Figure S7). The results show that  $\mathrm{Au}_{25}(\mathrm{SR})_{18}^-$  (2.15 mF cm<sup>-2</sup>) and  $\mathrm{Au}_{38}(\mathrm{SR})_{24}$  (2.27 mF cm<sup>-2</sup>) have similar active surface areas, which is consistent with our HER voltammograms and DFT calculations (Figure 3a/c, green/black lines). By contrast,  $\mathrm{Au}_{36}\mathrm{Ag}_2(\mathrm{SR})_{18}$  shows a much larger ECSA (3.86 mF cm<sup>-2</sup>) than those of the monomeric- $I_{\rm h}$  and dimeric- $I_{\rm h}$  counterparts (Figure S7d), hence, providing a direct evidence that the much improved HER of  $\mathrm{Au}_{36}\mathrm{Ag}_2(\mathrm{SR})_{18}$  is related to its trimeric- $I_{\rm h}$  structure with a larger active surface area or lower ligand coverage (*vide infra*).

The stability test was performed by cycling the catalyst 1000 times within 0.1~V to -0.6~V (Figure 3a, red dot line). The voltammetry curves before and after the stability test prove the high stability of our catalyst.

The most feasible active sites for H adsorption are found to be the kernel's shell Au atoms, i.e.,  $Au_{12}$  shell for  $Au_{25}(SR)_{18}$ ,  $Au_{21}$  shell for  $Au_{38}(SR)_{24}$ ,  $^{19,34}$  and  $Au_{27}Ag_2$  shell for  $Au_{36}Ag_2(SR)_{18}$  (Figure 3d). The optimized structures of the three NCs with one H adsorbed on the kernel's shell are shown in Figure 3e, where the H attaches to an atom of the  $I_h$ 

Au<sub>12</sub> shell in Au<sub>25</sub>(SCH<sub>3</sub>)<sub>18</sub> (Figure 3e, left); <sup>19,34</sup> for Au<sub>38</sub>(SCH<sub>3</sub>)<sub>24</sub>, the hydrogen binds at the bridging site of two fused icosahedrons (Figure 3e, middle), <sup>19</sup> whereas the HER active site on Au<sub>36</sub>Ag<sub>2</sub>(SCH<sub>3</sub>)<sub>18</sub> is any of the exposed Au on each  $I_h$  (Figure 3e, right). Note that due to the high symmetry of these NCs, beside the selected positions shown in Figure 3e, other sites can also form \*H with similar energies and thus constitute active sites. Typically, the number of surface atoms required to adsorb hydrogen<sup>34</sup> is similar for most Au<sub>n</sub>(SR)<sub>m</sub> NCs from small to large size. With the same mass (0.5 mg) of NCs, the surface atoms ( $N_{\rm surf.} = 8.46 \times 10^{17}$ ) for the tri- $I_h$  Au<sub>27</sub>Ag<sub>2</sub> shell of Au<sub>36</sub>Ag<sub>2</sub>(SR)<sub>18</sub> is much higher than 5.87 × 10<sup>17</sup> for the bi- $I_h$  Au<sub>12</sub> shell of Au<sub>38</sub>(SR)<sub>24</sub> and 4.89 × 10<sup>17</sup> for the mono- $I_h$  Au<sub>12</sub> shell of Au<sub>25</sub>(SR)<sub>18</sub> (Figure S8).

The higher HER activity of Au<sub>36</sub>Ag<sub>2</sub>(SR)<sub>18</sub> is also related to its greater negative electron affinity (Au<sub>36</sub>Ag<sub>2</sub>(SCH<sub>3</sub>)<sub>18</sub>, EA = -2.65 eV, compared to  $Au_{25}(SCH_3)_{18}^-$  with EA = 0.41 eV, and  $Au_{38}(SCH_3)_{24}$  with EA = -2.31 eV), implying more favorable electron acceptance, which in turn can be crucial for the first reaction step involving proton coupled electron transfer (Volmer step,  $H^+ + e^- + * \rightarrow *H$ ). The electron affinity trend of the three NCs is consistent with their corresponding LUMO state energies (Figures S4a and S6). We correlate the favorable electron affinity of Au<sub>36</sub>Ag<sub>2</sub>(SR)<sub>18</sub> to its unfilled supermolecular orbitals, i.e., the electronic shell closing trimeric supermolecule would have 24e distributed in 12 MOs (which originate from 1S1P (4 AOs) of each I<sub>h</sub> unit), but Au<sub>36</sub>Ag<sub>2</sub>(SR)<sub>18</sub> has only 20e, leaving two supermolecular orbitals being empty to accept electron(s) upon applied voltage, hence enhancing the catalytic activity. Note that Au<sub>38</sub>(SR)<sub>24</sub>, resembling a disuperatomic supermolecule, also has an empty supermolecular orbital<sup>35</sup> and EA slightly lower than Au<sub>36</sub>Ag<sub>2</sub>(SR)<sub>18</sub>; however, the energy for \*H adsorption on Au<sub>38</sub>(SCH<sub>3</sub>)<sub>24</sub>, i.e., the energy difference between the catalyst with and without a \*H, is very positive and offsets such an advantage, resulting in high  $\Delta G$  (Figure 3c). DFT calculations also indicate that the hypothetical trimeric Au<sub>38</sub>(SCH<sub>3</sub>)<sub>18</sub> (replacing the central Ag<sub>2</sub> with Au<sub>2</sub>) would be even better as HER catalyst due to its even lower \*H bonding energy of 0.63 eV and even higher EA of -2.77 eV. We further probe the HOMO and LUMO of the two NCs to understand the \*H bonding. Although there is no significant hybridization of the \*H atomic orbitals in the HOMO of both hypothetical  $Au_{38}(SCH_3)_{18}$  and experimental  $Au_{36}Ag_2(SCH_3)_{18}$  (Figure S9, bottom row, denoted by the black arrow), a considerable hybridization is observed in the LUMO of Au<sub>38</sub>(SCH<sub>3</sub>)<sub>18</sub> (Figure S9, top left), but hybridization is absent in that of Au<sub>36</sub>Ag<sub>2</sub>(SCH<sub>3</sub>)<sub>18</sub> (Figure S9, top right, indicated by red circle). Such hybridization differences result in the lower \*H bonding energy on Au<sub>38</sub>(SR)<sub>18</sub> compared to Au<sub>36</sub>Ag<sub>2</sub>(SCH<sub>3</sub>)<sub>18</sub>. However, there is no success yet in the synthesis of  $Au_{38}(SR)_{18}$ .

One may argue that, compared to  $Au_{25}(SC_2H_4Ph)_{18}$  and  $Au_{38}(SC_2H_4Ph)_{24}$ , the different ligand on  $Au_{36}Ag_2(SC_{10}H_{15})_{18}$  might also be responsible for the high HER performance. This is not the case, because the adamantanethiolate ligand on  $Au_{36}Ag_2$  is actually much bulkier at the Au-S interface than the  $SC_2H_4Ph$  ligand on  $Au_{25}$  and  $Au_{38}$  and thus would decrease the catalytic activity, but  $Au_{36}Ag_2(SR)_{18}$  instead shows the best activity in the series. Overall, even with the adverse effects of the adamantanethiolate,  $Au_{36}Ag_2(SR)_{18}$  still shows much higher catalytic activity than the other two NCs in the series,

indicating the dominant roles of geometrical and electronic effects of the metal core.

Low Ligand Coverage and Low-Coordinated Au Atoms. Although the number of kernel atoms increases from bi- $I_h$  Au<sub>2</sub>@Au<sub>21</sub> in Au<sub>38</sub>(SR)<sub>24</sub> to tri- $I_h$  Au<sub>3</sub>@Au<sub>27</sub>Ag<sub>2</sub> in Au<sub>36</sub>Ag<sub>2</sub>(SR)<sub>18</sub>, the total metal number in Au<sub>36</sub>Ag<sub>2</sub>(SR)<sub>18</sub> does not change compared to Au<sub>38</sub>(SR)<sub>24</sub>. Interestingly, Au<sub>36</sub>Ag<sub>2</sub>(SR)<sub>18</sub> has a much smaller number of ligands (18 only), being the same as that of Au<sub>25</sub>(SR)<sub>18</sub> (Figure 4, inset).

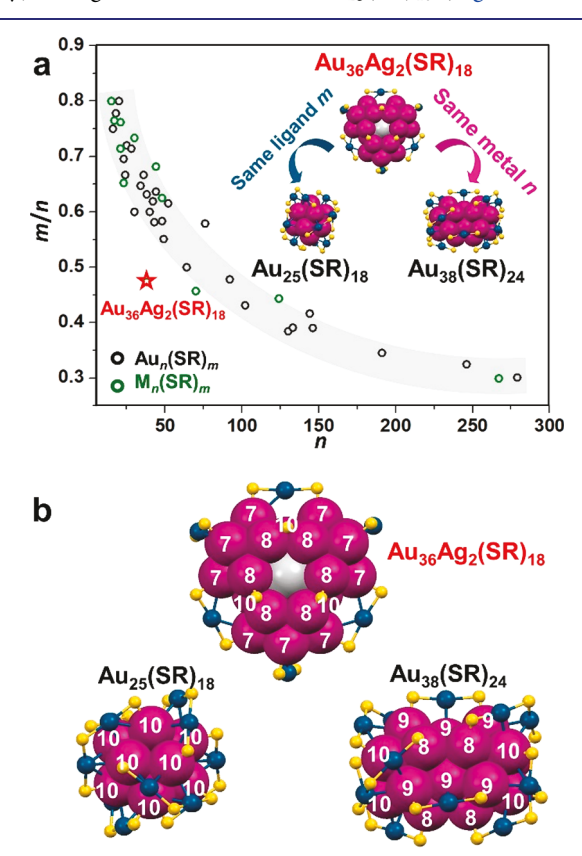


**Figure 4.** (a) The plot of ligand/metal number ratio (m/n) versus metal number (n). (b) The coordination numbers of Au atoms on the kernel's surface of  $Au_{36}Ag_2(SR)_{18}$ ,  $Au_{25}(SR)_{18}$ , and  $Au_{38}(SR)_{24}$ .

As a result, the thiolate coverage becomes much lower on  $\mathrm{Au_{36}Ag_2(SR)_{18}}$  (18/38 = 0.47). The plot summarizes the ligand coverages for the reported homogold  $\mathrm{Au}_n(SR)_m$  and  $\mathrm{Aubased}$  alloy  $\mathrm{Au}_{n-x}\mathrm{M}_x(SR)_m$  (M =  $\mathrm{Ag/Cu/Cd}$ ) NCs of atomic precision (Figure 4/Table S2). One can see that all of the previous  $\mathrm{Au}_n(SR)_m$  and  $\mathrm{Au}_{n-x}\mathrm{M}_x(SR)_m$  are located within the gray belt, indicating common ligand coverages based on the metal atom numbers. However, the new  $\mathrm{Au_{36}Ag_2(SR)_{18}}$  deviates significantly from the common ratios at the same metal number (n). The bulky adamantanethiolate ligand is crucial in the formation of the unique trimetric- $I_h$  kernel of  $\mathrm{Au_{36}Ag_2(SR)_{18}}$ . It is worth noting that other bulky ligands were also used previously to reduce the ligand coverage on Au NCs.  $^{37,38}\mathrm{Our}$  current work demonstrates the promise of the ligand strategy for designing effective HER catalysts.

This feature of low ligand coverage is important for the high HER activity of Au<sub>36</sub>Ag<sub>2</sub>(SR)<sub>18</sub>, as it relates to the lower coordination number of the metal atoms on the active site, which is critical for enhancing HER on Au nanocatalysts.<sup>39</sup> For example, laser-generated high density of stacking faults make

Ag NPs more active in HER catalysis due to the metal site's lower coordination. 40 Our approach of atomically precise nanochemistry further controls the distribution of lowcoordination sites even when the sizes (number of metal atoms) of catalysts are the same. As to Au NCs, doping Ag into the Au<sub>12</sub> shell in Au<sub>25-x</sub>Ag<sub>x</sub>(SR)<sub>18</sub><sup>-</sup> ( $x \sim 4.5$ ), however, resulted in deteriorated HER performance compared to homogold counterpart.<sup>20</sup> Although the central Ag atoms in Au<sub>36</sub>Ag<sub>2</sub>(SR)<sub>18</sub> have high coordination numbers (adverse for \*H adsorption), most of the Au atoms on the Au<sub>27</sub>Ag<sub>2</sub> shell are only 7 or 8 coordinated (both neighboring metal and S atoms counted) as indicated by SCXRD (Figure 4b, top), hence, favoring H adsorption. By contrast, the coordination number for each of the 12 Au shell atoms in  $\mathrm{Au}_{25}(\mathrm{SR})_{18}^-$  is 10, and that of the  $Au_{21}$  shell atoms in  $Au_{38}(SR)_{24}$  is 8 to 10 (Figure 4b, bottom). Thus, low coordinated Au atoms on Au<sub>36</sub>Ag<sub>2</sub>(SR)<sub>18</sub> also explain its much-improved H2 generation by lowering the adsorption energy barrier.

### CONCLUSIONS

Although Au and Ag have long been known as poor electrocatalysts for HER, our work demonstrates that tailoring of the geometrical and electronic structures can turn the particles into highly active HER catalysts. Specifically, a trimeric Au<sub>36</sub>Ag<sub>2</sub>(SR)<sub>18</sub> NC is obtained, and its structure exhibits three I<sub>h</sub> units face-fused together in the kernel. This NC can be regarded as a trimeric supermolecule with 20e (rather than the commonly observed  $3 \times 8e = 24e$ ) and thus exhibits two empty supermolecular orbitals. DFT calculations reveal that the binding energy of H on the active site of  $Au_{36}Ag_2(SR)_{18}$  is >0.45 eV lower than those of  $Au_{25}(SR)_{18}$  and  $Au_{38}(SR)_{24}$  in the series, and its electron affinity is also higher. The high activity of Au<sub>36</sub>Ag<sub>2</sub>(SR)<sub>18</sub> originates from several distinct factors: (1) more active sites on the NC surface for H adsorption; (2) the extraordinarily low ligand-to-metal ratio leads to exposure of low-coordinated surface Au atoms for H coordination; (3) the unfilled supramolecular orbital for easier electron acceptance from the electrode and thus faster electron transfer; (4) compared to other Au NCs, the lower H binding energy (related to the lower coordination number of Au atoms) and higher electron affinity (related to more negative LUMO) for an energetically feasible HER pathway. Overall, this work opens a new strategy for nanocatalyst design by tailoring the geometrical and electronic structures of metal NCs at the atomically precise level for customized applications.

## ASSOCIATED CONTENT

## Supporting Information

The Supporting Information is available free of charge at https://pubs.acs.org/doi/10.1021/jacs.1c04606.

Details of synthesis, characterizations, including MS, X-ray crystallography, electrochemical measurements details, computational details, and KS orbital analysis (PDF)

## **Accession Codes**

CCDC 2081877 contains the supplementary crystallographic data for this paper. These data can be obtained free of charge via <a href="https://www.ccdc.cam.ac.uk/data\_request/cif">www.ccdc.cam.ac.uk/data\_request/cif</a>, or by emailing data\_request@ccdc.cam.ac.uk, or by contacting The Cambridge Crystallographic Data Centre, 12 Union Road, Cambridge CB2 1EZ, UK; fax: +44 1223 336033.

#### AUTHOR INFORMATION

#### **Corresponding Authors**

Rongchao Jin — Department of Chemistry, Carnegie Mellon University, Pittsburgh, Pennsylvania 15213, United States; orcid.org/0000-0002-2525-8345; Email: rongchao@andrew.cmu.edu

Giannis Mpourmpakis — Department of Chemical Engineering, University of Pittsburgh, Pittsburgh, Pennsylvania 15261, United States; oocid.org/0000-0002-3063-0607; Email: gmpourmp@pitt.edu

Yongbo Song — Department of Chemistry, Carnegie Mellon University, Pittsburgh, Pennsylvania 15213, United States; School of Biomedical Engineering, Research and Engineering Center of Biomedical Materials, Anhui Medical University, Hefei, Anhui 230032, China; Email: ybsong860@ ahmu.edu.cn

#### **Authors**

**Yingwei Li** — Department of Chemistry, Carnegie Mellon University, Pittsburgh, Pennsylvania 15213, United States; orcid.org/0000-0002-4813-6009

Site Li — Department of Chemistry, Carnegie Mellon University, Pittsburgh, Pennsylvania 15213, United States; orcid.org/0000-0002-7221-1814

Anantha V. Nagarajan – Department of Chemical Engineering, University of Pittsburgh, Pittsburgh, Pennsylvania 15261, United States

**Zhongyu Liu** — Department of Chemistry, Carnegie Mellon University, Pittsburgh, Pennsylvania 15213, United States; orcid.org/0000-0002-2777-8360

Sarah Nevins – Department of Chemistry, Carnegie Mellon University, Pittsburgh, Pennsylvania 15213, United States

Complete contact information is available at: https://pubs.acs.org/10.1021/jacs.1c04606

#### **Author Contributions**

<sup>5</sup>These authors contribute equally to the work.

#### Notes

The authors declare no competing financial interest.

## **■** ACKNOWLEDGMENTS

R.J. acknowledges financial support from the National Science Foundation (NSF) under Grant No. DMR-1808675. G.M. acknowledges financial support from the U.S. Department of Energy, National Energy Technology Laboratory through NETL-Penn State University Coalition for Fossil Energy Research (UCFER, contract number DE-FE0026825). The authors would like to acknowledge computational support from the Center for Research Computing at the University of Pittsburgh and the National Energy Research Scientific Computing Center (NERSC), a U.S. Department of Energy Office of Science User Facility operated under contract no. DE-AC02-05CH11231.

## REFERENCES

(1) Gilroy, K. D.; Ruditskiy, A.; Peng, H.-C.; Qin, D.; Xia, Y. Bimetallic Nanocrystals: Syntheses, Properties, and Applications. *Chem. Rev.* **2016**, *116*, 10414–10472.

(2) Xie, C.; Niu, Z.; Kim, D.; Li, M.; Yang, P. Surface and Interface Control in Nanoparticle Catalysis. *Chem. Rev.* **2020**, *120*, 1184–1249. (3) Zhu, J.; Hu, L.; Zhao, P.; Lee, L. Y. S.; Wong, K.-Y. Recent Advances in Electrocatalytic Hydrogen Evolution Using Nanoparticles. *Chem. Rev.* **2020**, *120*, 851–918.

- (4) Jaramillo, T. F.; Jørgensen, K. P.; Bonde, J.; Nielsen, J. H.; Horch, S.; Chorkendorff, I. Identification of Active Edge Sites for Electrochemical H<sub>2</sub> Evolution from MoS<sub>2</sub> Nanocatalysts. *Science* **2007**, 317, 100–102.
- (5) Popczun, E. J.; McKone, J. R.; Read, C. G.; Biacchi, A. J.; Wiltrout, A. M.; Lewis, N. S.; Schaak, R. E. Nanostructured Nickel Phosphide as an Electrocatalyst for the Hydrogen Evolution Reaction. *J. Am. Chem. Soc.* **2013**, *135*, 9267–9270.
- (6) Kibsgaard, J.; Jaramillo, T. F.; Besenbacher, F. Building an Appropriate Active-Site Motif into a Hydrogen-Evolution Catalyst with Thiomolybdate  $[Mo_3S_{13}]^{2-}$  Clusters. *Nat. Chem.* **2014**, *6*, 248–253.
- (7) Mahmood, J.; Li, F.; Jung, S.-M.; Okyay, M. S.; Ahmad, I.; Kim, S.-J.; Park, N.; Jeong, H. Y.; Baek, J.-B. An Efficient and pH-Universal Ruthenium-Based Catalyst for the Hydrogen Evolution Reaction. *Nat. Nanotechnol.* **2017**, *12*, 441–446.
- (8) Faber, M. S.; Jin, S. Earth-Abundant Inorganic Electrocatalysts and Their Nanostructures for Energy Conversion Applications. *Energy Environ. Sci.* **2014**, *7*, 3519–3542.
- (9) Seh, Z. W.; Kibsgaard, J.; Dickens, C. F.; Chorkendorff, I.; Nørskov, J. K.; Jaramillo, T. F. Combining Theory and Experiment in Electrocatalysis: Insights into Materials Design. *Science* **2017**, 355, No. eaad4998.
- (10) Jin, R.; Zeng, C.; Zhou, M.; Chen, Y. Atomically Precise Colloidal Metal Nanoclusters and Nanoparticles: Fundamentals and Opportunities. *Chem. Rev.* **2016**, *116*, 10346–10413.
- (11) Li, Y.; Higaki, T.; Du, X.; Jin, R. Chirality and Surface Bonding Correlation in Atomically Precise Metal Nanoclusters. *Adv. Mater.* **2020**, 32, 1905488.
- (12) Jin, R.; Li, G.; Sharma, S.; Li, Y.; Du, X. Toward Active-Site Tailoring in Heterogeneous Catalysis by Atomically Precise Metal Nanoclusters with Crystallographic Structures. *Chem. Rev.* **2021**, *121*, 567–648.
- (13) Li, Y.; Jin, R. Seeing Ligands on Nanoclusters and in Their Assemblies by X-Ray Crystallography: Atomically Precise Nanochemistry and Beyond. *J. Am. Chem. Soc.* **2020**, *142*, 13627–13644.
- (14) Kang, X.; Zhu, M. Tailoring the Photoluminescence of Atomically Precise Nanoclusters. *Chem. Soc. Rev.* **2019**, 48, 2422–2457.
- (15) Zeng, C.; Chen, Y.; Kirschbaum, K.; Lambright, K. J.; Jin, R. Emergence of Hierarchical Structural Complexities in Nanoparticles and Their Assembly. *Science* **2016**, *354*, 1580–1584.
- (16) Zhuang, S.; Chen, D.; Liao, L.; Zhao, Y.; Xia, N.; Zhang, W.; Wang, C.; Yang, J.; Wu, Z. Hard-Sphere Random Close-Packed Au<sub>4</sub>, Cd<sub>2</sub>(TBBT)<sub>31</sub> Nanoclusters with a Faradaic Efficiency of Up to 96% for Electrocatalytic CO<sub>2</sub> Reduction to CO. *Angew. Chem., Int. Ed.* **2020**, 59, 3073–3077.
- (17) Zhou, M.; Higaki, T.; Hu, G.; Sfeir, M. Y.; Chen, Y.; Jiang, D.; Jin, R. Three-Orders-of-Magnitude Variation of Carrier Lifetimes with Crystal Phase of Gold Nanoclusters. *Science* **2019**, *364*, 279–282.
- (18) Kwak, K.; Choi, W.; Tang, Q.; Kim, M.; Lee, Y.; Jiang, D.; Lee, D. A Molecule-Like PtAu<sub>24</sub>(SC<sub>6</sub>H<sub>13</sub>)<sub>18</sub> Nanocluster as An Electrocatalyst for Hydrogen Production. *Nat. Commun.* **2017**, *8*, 14723.
- (19) Choi, W.; Hu, G.; Kwak, K.; Kim, M.; Jiang, D.; Choi, J.-P.; Lee, D. Effects of Metal-Doping on Hydrogen Evolution Reaction Catalyzed by  $MAu_{24}$  and  $M_2Au_{36}$  Nanoclusters (M = Pt, Pd). ACS Appl. Mater. Interfaces **2018**, 10, 44645–44653.
- (20) Kumar, B.; Kawawaki, T.; Shimizu, N.; Imai, Y.; Suzuki, D.; Hossain, S.; Nair, L. V.; Negishi, Y. Gold Nanoclusters as Electrocatalysts: Size, Ligands, Heteroatom Doping, and Charge Dependences. *Nanoscale* **2020**, *12*, 9969–9979.
- (21) Shichibu, Y.; Negishi, Y.; Watanabe, T.; Chaki, N. K.; Kawaguchi, H.; Tsukuda, T. Biicosahedral Gold Clusters  $[\mathrm{Au}_{25}(\mathrm{PPh}_3)_{10}(\mathrm{SC}_n\mathrm{H}_{2n+1})_5\mathrm{Cl}_2]^{2+}$  (n=2-18): A Stepping Stone to Cluster-Assembled Materials. J. Phys. Chem. C 2007, 111, 7845–7847. (22) Jin, R.; Liu, C.; Zhao, S.; Das, A.; Xing, H.; Gayathri, C.; Xing, Y.; Rosi, N. L.; Gil, R. R.; Jin, R. Tri-Icosahedral Gold Nanocluster  $[\mathrm{Au}_{37}(\mathrm{PPh}_3)_{10}(\mathrm{SC}_2\mathrm{H}_4\mathrm{Ph})_{10}\mathrm{X}_2]^+$ : Linear Assembly of Icosahedral Building Blocks. ACS Nano 2015, 9, 8530–8536.

- (23) Zhou, M.; Jin, R.; Sfeir, M. Y.; Chen, Y.; Song, Y.; Jin, R. Electron Localization in Rod-Shaped Triicosahedral Gold Nanocluster. *Proc. Natl. Acad. Sci. U. S. A.* **2017**, *114*, E4697–E4705.
- (24) Teo, B. K.; Zhang, H. Polyicosahedricity: Icosahedron to Icosahedron of Icosahedra Growth Pathway for Bimetallic (Au—Ag) and Trimetallic (Au—Ag—M; M—Pt, Pd, Ni) Supraclusters; Synthetic Strategies, Site Preference, and Stereochemical Principles. *Coord. Chem. Rev.* 1995, 143, 611–636.
- (25) Peng, Y.; Liu, Q.; Lu, B.; He, T.; Nichols, F.; Hu, X.; Huang, T.; Huang, G.; Guzman, L.; Ping, Y.; Chen, S. Organically Capped Iridium Nanoparticles as High-Performance Bifunctional Electrocatalysts for Full Water Splitting in Both Acidic and Alkaline Media: Impacts of Metal-Ligand Interfacial Interactions. ACS Catal. 2021, 11, 1179—1188.
- (26) Zhu, M.; Aikens, C. M.; Hollander, F. J.; Schatz, G. C.; Jin, R. Correlating the Crystal Structure of a Thiol-Protected Au<sub>25</sub> Cluster and Optical Properties. *J. Am. Chem. Soc.* **2008**, *130*, 5883–5885.
- (27) Qian, H.; Eckenhoff, W. T.; Zhu, Y.; Pintauer, T.; Jin, R. Total Structure Determination of Thiolate-Protected Au<sub>38</sub> Nanoparticles. *J. Am. Chem. Soc.* **2010**, *132*, 8280–8281.
- (28) Li, Y.; Cowan, M. J.; Zhou, M.; Taylor, M. G.; Wang, H.; Song, Y.; Mpourmpakis, G.; Jin, R. Increasing the Dipole Moments of M<sub>23</sub> (M = Au/Ag/Cd) Nanoclusters by Heterometal-Doping. *ACS Nano* **2020**, *14*, 6599–6606.
- (29) Li, Y.; Luo, T.-Y.; Zhou, M.; Song, Y.; Rosi, N. L.; Jin, R. A Correlated Series of Au/Ag Nanoclusters Revealing the Evolutionary Patterns of Asymmetric Ag Doping. J. Am. Chem. Soc. 2018, 140, 14235–14243.
- (30) Li, Y.; Taylor, M. G.; Luo, T.-Y.; Song, Y.; Rosi, N. L.; Mpourmpakis, G.; Jin, R. Heteroatom Tracing Reveals the 30-Atom Au-Ag Bimetallic Nanocluster as a Dimeric Structure. *J. Phys. Chem. Lett.* **2020**, *11*, 7307–7312.
- (31) Zhou, M.; Yao, C.; Sfeir, M. Y.; Higaki, T.; Wu, Z.; Jin, R. Excited-State Behaviors of M<sub>1</sub>Au<sub>24</sub>(SR)<sub>18</sub> Nanoclusters: The Number of Valence Electrons Matters. *J. Phys. Chem. C* **2018**, 122, 13435–13442.
- (32) Cheng, L.; Ren, C.; Zhang, X.; Yang, J. New Insight into the Electronic Shell of Au<sub>38</sub>(SR)<sub>24</sub>: A Superatomic Molecule. *Nanoscale* **2013**, *5*, 1475–1478.
- (33) Alfonso, D. R.; Kauffman, D.; Matranga, C. Active Sites of Ligand-Protected  $Au_{25}$  Nanoparticle Catalysts for  $CO_2$  Electroreduction to CO. *J. Chem. Phys.* **2016**, 144, 184705.
- (34) Hu, G.; Tang, Q.; Lee, D.; Wu, Z.; Jiang, D. Metallic Hydrogen in Atomically Precise Gold Nanoclusters. *Chem. Mater.* **2017**, *29*, 4840–4847.
- (35) Lopez-Acevedo, O.; Tsunoyama, H.; Tsukuda, T.; Häkkinen, H.; Aikens, C. M. Chirality and Electronic Structure of the Thiolate-Protected Au<sub>38</sub> Nanocluster. *J. Am. Chem. Soc.* **2010**, *132*, 8210–8218.
- (36) Taylor, M. G.; Mpourmpakis, G. Thermodynamic Stability of Ligand-Protected Metal Nanoclusters. *Nat. Commun.* **2017**, 8 (8), 15988.
- (37) Nishigaki, J.; Tsunoyama, R.; Tsunoyama, H.; Ichikuni, N.; Yamazoe, S.; Negishi, Y.; Ito, M.; Matsuo, T.; Tamao, K.; Tsukuda, T. A New Binding Motif of Sterically Demanding Thiolates on a Gold Cluster. *J. Am. Chem. Soc.* **2012**, *134*, 14295–14297.
- (38) Nishigaki, J.; Yamazoe, S.; Kohara, S.; Fujiwara, A.; Kurashige, W.; Negishi, Y.; Tsukuda, T. A Twisted Bi-Icosahedral Au<sub>25</sub> Cluster Enclosed by Bulky Arenethiolates. *Chem. Commun.* **2014**, *50*, 839–841.
- (39) Mistry, H.; Reske, R.; Zeng, Z.; Zhao, Z.-J.; Greeley, J.; Strasser, P.; Cuenya, B. R. Exceptional Size-Dependent Activity Enhancement in the Electroreduction of CO<sub>2</sub> over Au Nanoparticles. *J. Am. Chem. Soc.* **2014**, *136*, 16473–16476.
- (40) Li, Z.; Fu, J.-Y.; Feng, Y.; Dong, C.-K.; Liu, H.; Du, X.-W. A Silver Catalyst Activated by Stacking Faults for the Hydrogen Evolution Reaction. *Nat. Catal.* **2019**, *2*, 1107–1114.